Published online 21 January 2014 *Nucleic Acids Research, 2014, Vol. 42, No. 6* ***e49***
doi:10.1093/nar/gkt1404

Purification, characterization and crystallization of the human 80S ribosome

Heena Khatter, Alexander G. Myasnikov, Leslie Mastio, Isabelle M. L. Billas, Catherine Birck, Stefano Stella and Bruno P. Klaholz*

Centre for Integrative Biology (CBI), Department of Integrated Structural Biology, IGBMC (Institute of Genetics and of Molecular and Cellular Biology), Centre National de la Recherche Scientifique (CNRS) UMR 7104/Institut National de la Santé de la Recherche Médicale (INSERM) U964/Université de Strasbourg, 1 rue Laurent Fries, 67404 Illkirch, France

Received November 14, 2013; Accepted December 20, 2013

ABSTRACT

Ribosomes are key macromolecular protein synthesis machineries in the cell. Human ribosomes have so far not been studied to atomic resolution because of their particularly complex structure as compared with other eukaryotic or prokaryotic ribosomes, and they are difficult to prepare to high homogeneity, which is a key requisite for high-resolution structural work. We established a purification protocol for human 80S ribosomes isolated from HeLa cells that allows obtaining large quantities of homogenous samples as characterized by biophysical methods using analytical ultracentrifugation and multiangle laser light scattering. Samples prepared under different conditions were characterized by direct single particle imaging using cryo electron microscopy, which helped optimizing the preparation protocol. From a small data set, a 3D reconstruction at subnanometric resolution was obtained showing all prominent structural features of the human ribosome, and revealing a salt concentration dependence of the presence of the exit site tRNA, which we show is critical for obtaining crystals. With these well-characterized samples first human 80S ribosome crystals were obtained from several crystallization conditions in capillaries and sitting drops, which diffract to 26 Å resolution at cryo temperatures and for which the crystallographic parameters were determined, paving the way for future high-resolution work.

INTRODUCTION

Ribosomes are composed of two subunits, the large (60S/50S) and the small (40S/30S) ribosomal subunits, which assemble together to form the functional 80S and 70S in eukaryotes and prokaryotes, respectively. Each subunit has protein and ribosomal RNA (rRNA) components with a relatively stable rRNA/protein ratio of 2:1 in cytosolic mammalian and bacterial ribosomes. The overall structure of the ribosome is conserved in all species consisting of the three tRNA binding sites [aminoacyl (A), peptidyl (P) and exit (E)], the GTPase center and the peptidyl transferase center. However, apart from the conserved core, eukaryotic ribosomes are more complex and contain many more proteins (26 extra) and longer rRNA (including long expansion segments, ES) (1). These ES have been hypothesized to allow ribosome docking on the endoplasmic reticulum, possibly providing scaffolding sites to bind additional proteins and form eukaryote-specific inter-subunit bridges (2). Also, functionally, the eukaryotic ribosomes have many more factors involved in every step of translation (initiation, elongation, termination and recycling) reflecting a high level of regulation (3–6).

The crystal structures of eukaryotic ribosomes from *Saccharomyces cerevisiae* 80S at 3.0 Å (7), *Tetrahymena thermophila* 60S at 3.5 Å and 40S at 3.9 Å (8,9) have highlighted the additional protein and rRNA components and precisely assigned their positions. The more complex higher eukaryotic ribosomes have been extensively studied by single particle cryo electron microscopy (cryo-EM) providing the first structure of the wheat germ ribosome obtained at 38 Å (10), which recently reached 5.5 Å resolution (11). Cryo-EM maps for

*To whom correspondence should be addressed. Tel: +33 388655755; Fax: +33 388653276; Email: klaholz@igbmc.fr
Present address:
Stefano Stella, Structural Biology and Biocomputing Programme, Centro Nacional de Investigaciones Oncológicas, C/Melchor Fernández Almagro, 3, E-28029 Madrid, Spain.

mammalian ribosomes such as canine, human (HeLa cell) and rabbit ribosomes (12–15) are available at relatively low resolutions of 8–15 Å but were the pioneer studies that allowed localizing eukaryote-specific proteins such as RACK1, rpS27e, rpS25e, rpL30e (16,17). Recently, the cryo-EM structures of human and drosophila ribosomes were elucidated in more detail with a resolution range of 5–9 Å, with the latest structure of the human ribosome reaching the 4–5 Å range (18). The availability of only a handful of eukaryotic ribosome structures (19–22) emphasizes the difficulty of appropriate purification, the limiting point being the availability of homogenous samples in large quantities required both for cryo-EM and crystallography.

Studying human ribosomes as opposed to ribosomes from other species is crucially important for understanding the mechanism of antibiotic action and selectivity with respect to ribosomes from various pathogenic bacteria, an ever increasing problem with the constantly growing occurrence of antibiotic resistance (23,24). The previous structures of prokaryotic ribosomes with antibiotics like paramomycin, streptomycin, tetracycline, hygromycin B, etc. have helped to elucidate the structural basis for their efficacy (25,26) and the species-specific interactions between ribosomes and antibiotics (27,28). Obtaining accurate information on the human ribosome would provide a prospect of developing specific antibiotics preferentially targeting the function of the prokaryotic ribosome with improved efficiency and reduced side effects, i.e. provide the molecular basis of cross-reactivity of existing or future antibiotics, which would be useful for the discovery of novel antibiotics. Human ribosomes have been purified earlier, from HeLa cells and placenta or blood (18,29) as separate subunits and reconstituted to 80S (30) for biochemical and cryo-EM analysis. However, to our knowledge, they have not yet been crystallized in the form of the fully assembled, endogenous 80S complex, which would be a key advance to get atomic level information. This would be crucial in particular for antibiotic complexes to understand the binding of those ligands that induce side effects, and of other and future drugs targeting the human ribosome (as accompanying drugs to reduce cellular activity such as required in the case of the treatment of cancer). Here, we establish a protocol to purify 80S ribosomes from HeLa cells in large amounts and describe the sample optimization by monitoring the homogeneity through sucrose gradients, Analytical Ultracentrifugation (AUC), Size Exclusion Chromatography Multiangle Laser Light Scattering (SEC-MALLS) and cryo-EM, which allowed obtaining crystallizable material. The crystals obtained here were characterized at synchrotron X-ray sources with respect to their crystallographic parameters such as cell parameters, space group, solvent content, etc., which represents essential information for future high-resolution work using crystallography.

MATERIALS AND METHODS

Detailed protocol of ribosome purification from HeLa cells

Equipments required: 10-l flasks for cell culture, SW-28 rotor, Type 50.2 Ti Beckman-Coulter rotor, GE SG-50 Gradient maker, Econo UV Monitor (Biorad), a Fraction Collector (Biorad), Econo Gradient Pump (Biorad).

Deionized distilled water is used for buffer preparations, and complete protease inhibitor (Roche) is added to all the buffers. Also, sucrose solution must be treated with bentonite after preparation with buffer A to inhibit ribonucleases (31,32) if present. Buffer A contains 20 mM Tris, pH 7.5, 2 mM $Mg(OAc)_2$, 150 mM KCl. Buffer B contains 20 mM Tris, pH 7.5, 6 mM $Mg(OAc)_2$, 150 mM KCl, 6.8% sucrose, 1 mM DTT, RNasin Plus RNase Inhibitor (Promega). Resuspension buffer C contains 100 mM KCl, 5 mM $Mg(OAc)_2$, 20 mM HEPES, pH 7.6, 1 mM DTT, 10 mM NH_4Cl. For 60S and 40S subunit purification a slightly modified buffer A is required containing 20 mM Tris, pH 7.5, 2 mM $Mg(OAc)_2$, 500 mM KCl. The role of ion concentration in inter- and intra-subunit interaction is discussed in the 'Results' section.

Step 1: HeLa cell preparation

HeLa cells are grown in suspension cultures (55×10^8 cells, ~6 l) in Minimal Essential Media Spinner Modification (S-MEM; Sigma Aldrich) supplemented with 7% newborn calf serum, 2 mM Glutamine and 40 μg/ml gentamycin at 37°C in 5% CO_2 environment. Once confluent, they are serum-starved for 6 h to get a synchronized cell population.

Step 2: Lysis and sucrose cushion

Cells are then lysed in freshly prepared lysis buffer containing 15 mM Tris, pH 7.5, 0.5% NP40 (Sigma-Aldrich), 6 mM $MgCl_2$, 300 mM NaCl, RNAsin (Promega). After 30 min incubation on ice, the lysate is centrifuged at 12 000*g* for 10 min to remove debris, nuclei and mitochondria (33). The supernatant is loaded on 30% sucrose cushion prepared in Buffer A and centrifuged for 16 h at 115 800*g* (50.2 Ti rotor) to get the crude ribosomal pellet (29,30). While loading the cushion, care must be taken to not disturb the sucrose, and ensure slow addition of the lysate to the 30% sucrose. This pellet is resuspended in Buffer B to homogeneity. The presence of nonresuspended particles in this solution can affect the next step, and these particles must be removed by a short centrifugation (10 min at 10 000*g*). Only the supernatant is used for the next step.

Step 3: Sucrose density gradient

Gradient preparation: SG 50 Gradient Maker (GE Healthcare) is used to make a linear gradient of 15–30%, wherein the higher % sucrose solution is loaded in the mixing chamber and the lower % sucrose solution is loaded in the other, allowing to mix slowly. The outlet is

connected with a pump and sucrose is collected drop wise from the outlet.

The supernatant is treated with 1 mM puromycin for 30 min at 4°C (34) with intermittent mixing and loaded on 15–30% sucrose gradient prepared in Buffer A. The samples are centrifuged at 25 000 rpm for 11 h in a SW-28 rotor and fractions are collected from bottom to top using an Econo Gradient Pump (Biorad) with an Econo UV Monitor (Biorad) and a Fraction Collector. The sample absorbance is recorded using UV reader (Biorad) and the peak corresponding to 80S is pooled for PEG20K precipitation (7). A final concentration of 7% PEG20K is added to the pooled fractions, incubated on ice for 10 min and centrifuged at 17 400*g* for 10 min. The pure ribosomal pellet is dissolved in resuspension buffer C and filtered using 0.22 µm filters (Millipore) for further analysis or stored without filtration on ice for 7 days for crystallization. Snap freezing and storage is not advised. For concentration calculations, 1 A_{260} unit corresponds to 20 pmol of 80S ribosome.

Analytical ultracentrifugation

Sedimentation velocity experiments were conducted using Beckman Coulter ProteomeLab XL-I analytical ultracentrifuge using the 8-hole Beckman An-50Ti rotor at 4°C for samples in resuspension buffer (35). Sedimentation at 15 000 rpm was monitored by absorbance at 280 nm with scans made at 4 min intervals. The solution density and viscosity for resuspension buffer were calculated using SEDNTERP software. Data were analyzed using a c(s) model in SEDFIT (Figure 1) (36).

Size exclusion chromatography multiangle laser light scattering

The molecular weight and homogeneity of the sample was checked using a SEC column coupled with MALLS Dawn DSP detector (Wyatt Technology, Santa Barbara, CA, USA) (Figure 1B). To prevent bacterial growth, 0.01% sodium azide was added to the resuspension buffer, which was then filtered through 0.25 µm filter membranes (Millipore) before equilibrating the Superdex 200 10/300 analytical column (GE healthcare life sciences). The system was operated at 20°C, with a flow rate of 0.75 ml/min.

Single-particle cryo-EM

For cryo-EM analysis, 80S ribosome samples were deposited on Quantifoil 2/2 holey carbon film, blotted with a filter paper and flash-frozen [using FEI Vitrobot (Mark IV)] to obtain ribosomes embedded in a thin layer of vitreous ice suspended across the holes (Figure 2). The images were collected at liquid-nitrogen temperature using the in-house FEI Tecnai F30 (Polara) field emission gun (FEG) transmission cryo electron

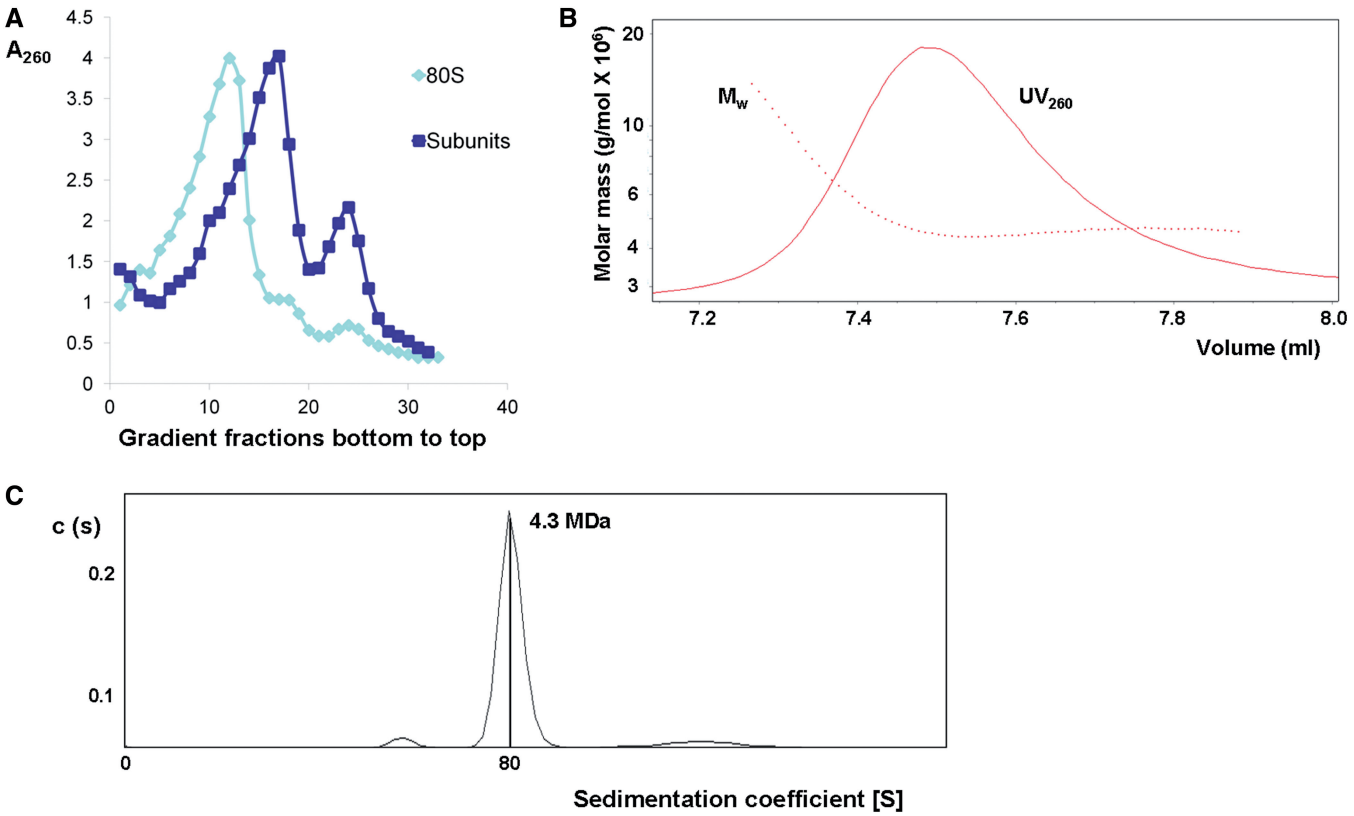

Figure 1. Biophysical characterization of human 80S ribosomes purified from HeLa cells. (**A**) 15–30% sucrose density gradient profiles for 80S, and dissociated 60S and 40S subunits depicting the separation of components based on density. (**B**) SEC-MALLS for 80S sample and (**C**) AUC results showing the homogeneity of 80S sample, which corresponds to the calculated molecular weight of 4.3 MDa.

Table 1. Experimental details of cryo-EM data collection

cryo-EM data collection	Empty 80S ribosome	80S ribosome with E-site tRNA
Detector	CCD Eagle 4 k × 4 k	CMOS Falcon 1 4 k × 4 k
Voltage	100 kV	300 kV
Pixel size	1.82 Å	1.14 Å
Box size	240 × 240	512 × 512
Magnification	59 k	93 k
Number of particles	15 000	24 000
Total dose	15 $\bar{e}$/Å^2	20 $\bar{e}$/Å^2
Defocus	−0.8 to −3.5 μm	−1 to −5 μm

microscope operating at 150 kV acceleration voltage with a dose of ~10–15 electrons per Å^2 at a magnification of 59 000 on a 4 k × 4 k CCD Eagle camera (FEI) resulting in a final step size of 1.82 Å per pixel. Another data set was collected at 150 kV acceleration voltage with magnification of 93 000 on a CMOS Falcon 1 camera (FEI; installed as an upgrade on the microscope while this work was ongoing) resulting in a final step size of 1.14 Å per pixel (Table 1). Automatic image acquisition was performed using EPU software (FEI). After visual inspection only images with best power-spectra were selected for image processing. Particle selection was done semi-automatically in e2boxer.py (EMAN2) with validation of all boxed particles by visual inspection. Defocus value estimation and contrast transfer function correction by phase flipping were done by using the program 2ctf.py from the EMAN2 software package (37,38). Structure determination and refinement was done using the EMAN2 software packages (37,38). The resolution of the final 3D structures was estimated by Fourier Shell Correlation (39) according to the 0.5, 0.14 (40) and one-half-bit (41) criteria to 13.3, 8.7 and 9.3 Å for the empty ribosome consistent with the features of the maps, while it was 16.5, 11.7 and 11.5 Å for ribosome with E-site tRNA, respectively.

Crystallization of human 80S ribosomes

The purified 80S ribosomes were filtered using Millipore 0.22 μm after 7 days of annealing on ice [as for yeast ribosomes; (7)], and the sample was kept at room temperature for an hour before setting up crystallization screens. Purified ribosomes (0.35 μl) at 5–9 mg/ml were loaded on one side of The Crystal Former (Microlytic) and 0.35 μl of precipitant were loaded on the other side. A number of screens were tested including PEGs (Hampton Research), PEG-Ion pH (Hampton Research), Nucleix (Qiagen) and Protein Complex (Qiagen) at 4 and 17°C. Microcrystals were obtained with 20% PEG 10 K, 100 mM Na HEPES, pH 7.5, or with 15% PEG 20K, 100 mM Na HEPES, pH 7.5, at 17°C (Figure 3A). Optimization of the crystallization conditions with 30% PEG 20 K, 10 mM $Mg(OAc)_2$ and 100 mM Na-HEPES, pH 7.5, allowed obtaining slightly larger crystals. Apart from the crystal former, also the crystal Harp (Molecular Dimensions) and classical glass capillaries of 0.5 and 1 mm were tested. These crystals could not be directly reproduced in sitting drops (with 1:1 sample/precipitant) with the same conditions. Therefore, in a concentration range of 5–9 mg/ml of purified ribosomes, optimization of the PEG 20K concentration and other condition with PEG 10K as precipitant, was done to get crystals in sitting drops. This included commercial screens such as PEGs (Hampton Research), PEG-Ion pH (Hampton Research), Nucleix (Qiagen) and Protein Complex (Qiagen). Plate-like crystals were obtained with 2 μl of 8 mg/ml of sample mixed with 2 μl of 4% PEG 20 K, 100 mM Na-HEPES, pH 7.5, and 50 mM KSCN. Eighteen percent glycerol or a series of small PEGs such as 8% PEG 4K, 8% PEG 6K, 8% PEG 8K along with 8% glycerol as cryo-protectants were tested, with 18% glycerol alone being the best one found here.

RESULTS

Preparation and characterization of human 80S ribosomes

Because serum starvation is known to inhibit translation in eukaryotic cell lines (42), we reasoned that this may be a way to obtain more homogenous monosomes. HeLa cells were therefore grown in suspension balloons and serum-starved for 6 h or processed directly. Human 80S ribosomes were isolated from the cell lysate after centrifugation to remove mitochondria and nuclei, and the supernatant was loaded onto a 30% sucrose cushion. The pellet obtained was treated with puromycin to remove nascent peptides bound to the 80S, giving a yield of 7–8 mg of pure ribosomes from 6 l of cells ($20–25 \times 10^8$) after the sucrose gradient (29). The presence of 18S and 28S rRNAs was confirmed by ethidium bromide staining. Several steps had to be optimized during purification to ensure homogeneity of the sample to be used for structural studies. Cell lysis being the most important step due to the presence of numerous proteases was treated with the maximum precaution. Several detergents such as CHAPS, NP-40 and Triton X-100 were tried, also dounce homogenizer was used to see if cell disruption would work better. However, 0.5% NP-40 turned out to be the mildest procedure, as monitored by cryo-EM imaging of 80S particles. The other bottleneck was removal of sucrose, which is a basic necessity for EM to ensure a good image contrast (43). For this, different methods were tried such as (i) centrifugation of the sucrose gradient fractions and resuspension of the pellet, (ii) exchanging buffer with a NAP column and then concentrating the sample and (iii) PEG 20K precipitation. The fastest, most convenient and least influencing procedure on ribosome stability was precipitation using PEG 20K, a method also used for yeast ribosome purification (7). Salt composition and concentration (KCl and Mg^{2+}) were optimized using cryo-EM imaging (see below).

The presence of all ribosomal proteins was confirmed using mass spectrometry (Supplementary Tables 1 and 2). It can, however, not be excluded that some loosely bound ribosomal proteins are present with variable stoichiometry in the 80S complex because protein peptide fragment occurrence depends also on how well the proteins can be

digested and detected by mass spectrometry. The sample was analyzed by SEC-MALLS and AUC (Figure 1B and C). The sedimentation coefficient was determined to be close to 80S with a single major peak obtained in AUC corresponding to 4.3 MDa (the theoretical value is 4.2 MDa), a result consistent with the chromatogram from SEC-MALLS. While the precision of SEC-MALLS and AUC cannot address whether all ribosomes contain all ribosomal proteins because of the high molecular weight, these analytical techniques were useful to monitor the sample quality throughout the purification procedure.

Cryo electron microscopy

To evaluate the homogeneity and monodispersity of the 80S ribosomes, the particle distribution was analyzed under different preparation conditions using cryo-EM imaging (Figure 2). This helped in finding the optimal conditions for purification, the optimal buffer being 150 mM KCl and 5 mM Mg^{2+} or less. Buffers with higher Mg^{2+} concentration showed aggregation, while higher KCl concentration increasingly leads to the appearance of the individual ribosomal subunits. The role of monovalent and divalent cations on subunit association has been well documented for prokaryotes and to some extent for eukaryotes as well. Previously, the concentration of potassium and magnesium in the resuspension buffer was observed to be crucial (44,45). In our hands, the sample completely aggregates at 20 mM $Mg(OAc)_2$, while at 5 mM and below it is monodisperse, as can be judged from the even distribution of ribosome particles on a cryo-EM grid (Figure 2C). This is consistent with the cellular concentration of magnesium being around 1 mM, which would promote the ribosomes to remain monodisperse when not translating. In contrast, the potassium concentration was found to be critical for the association of the two ribosomal subunits (46). At 150 mM KCl, 80S ribosomes were found to be stable at a concentration that compares well with that in cells. Only at significantly higher salt concentrations such as 500 mM KCl, the subunits become dissociated on the sucrose density gradient (Figure 1A). Consistent with this observation is the idea that potassium is required for inter-subunit stability while magnesium ensures proper rRNA folding. However, at higher concentrations, magnesium promotes inter-particle contacts, which lead to ribosome aggregation and precipitation as visualized by cryo-EM imaging.

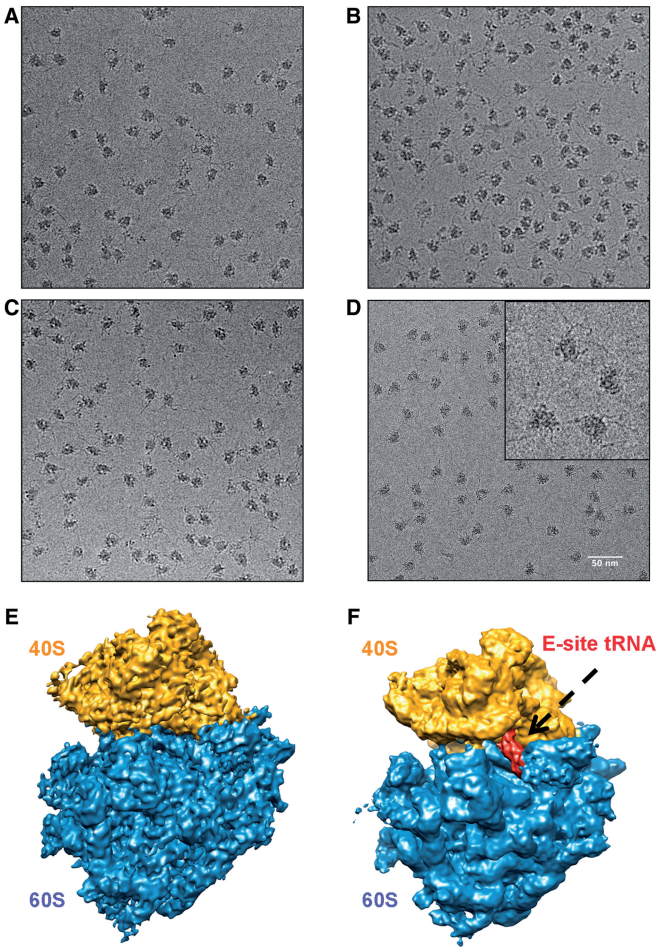

Figure 2. Cryo electron micrograph depicting the distribution of 80S particles at 59k magnification, collected using a Polara F-30 electron microscope. The ribosomes were isolated from Hela cells (**A**) under normal growth conditions (**B**) in stationary phase of growth (**C**) after glutamine starvation (**D**) after serum-starvation (inset shows the zoomed-in view for individual ribosomes). (**E**) The cryo-EM structure of empty human 80S and with (**F**) E-site tRNA; both isolated from HeLa cells; under high and low KCl concentration during Puromycin treatment, respectively; color code: 40S golden, 60S blue, tRNA red.

Using optimized buffers, single-particle cryo-EM data sets were collected for 80S samples obtained from serum-starved HeLa cell for two salt concentrations during Puromycin treatment (150 or 300 mM KCl). The serum starvation is an important step towards getting a clean homogenous sample as was observed from direct cryo-EM imaging. Ribosomes isolated from nonstarved cells show impurities (Figure 2A), while ribosomes isolated from cells in stationary phase appear to undergo partial degradation (Figure 2B; for these reasons 3D reconstructions were not attempted from these samples). Glutamine starvation also shows ribosomes with either partial degradation or with impurities (Figure 2C). Serum is known to affect translation because its absence reduces the rate of *in vitro* polypeptide synthesis. We observed that on serum starvation of HeLa cells for 6 h, which leads to cell synchronization, ribosomes appear to be more homogenous, as can be judged from the cryo-EM images (Figure 2D).

A 3D reconstruction obtained from only 15 000 particles of 80S ribosomes (serum-starved) already provides a well-defined structure of the human ribosome with all the major landmarks such as the L1 stalk, the central protuberance in the large subunit and the head, beak, body and feet in the small subunit (Figure 2E). These features are consistent with the human ribosome structure published in previous studies (13,47). This 80S structure was obtained from ribosomes that went through a high-salt (300 mM) washing step during puromycin treatment right after the sucrose cushion. Next, to keep the salt concentration constant throughout the purification process, we decided to skip the high-salt washing step and maintain 150 mM KCl throughout.

Interestingly, the cryo-EM reconstruction from such samples reveals the presence of an E-site tRNA (Figure 2F), a well-defined L1 stalk next to the E-site tRNA and well-ordered P-proteins (these regions are largely disordered in the high-salt washed ribosomes). This shows that the absence of a high-salt step allows maintaining an endogenous tRNA in the E-site, while mRNA and peptide are absent as revealed by the comparison of the corresponding cryo-EM reconstructions. The lower resolution of the E-site tRNA complex as compared with that of the empty ribosome may be due to ribosome subpopulations with different conformations, which would be compatible with the observation of different conformations in the asymmetric unit of yeast (7) and *T. thermophila* ribosomes (48).

Crystallization of the human 80S ribosome

The high homogeneity of the sample allowed us obtaining crystals in the microlytic crystal former capillaries as well as in a crystal harp, and also in sitting drops. After screening several conditions from PEGs (Hampton), PEG Ion pH (Hampton) and Protein complex (Qiagen) screens at 4 and 17°C, initial hits of microcrystals were obtained in capillaries with two conditions: 20% PEG 10K, 0.1 M Na HEPES, pH 7.5, and 15% PEG 20K, 0.1 M Na HEPES, pH 7.5, at 17°C. An increasing gradient of microcrystals (10–30 μm in size) could be observed from the precipitant loading side to the protein loading side. Optimization of the conditions provided larger crystals with 30% PEG 20K, 0.1 M Na HEPES, pH 7.5, and 10 mM $Mg(OAc)_2$ (Figure 3A). *In situ* diffraction from capillaries was attempted at the PX III beamline of the Swiss Light Source (SLS) synchrotron at room temperature as well as under cryo conditions (by freezing the tip of the capillary containing crystals, tested on beamline PX I). While no diffraction spots could be seen, this was a first indication that these crystals were not salt. However, owing to the complexity of handling them in capillaries they could not be mounted in loops. Direct freezing of capillaries was successful with respect to cryo conditions (no ice rings), but showed no diffraction (either no diffraction or high background due to the large mass of solvent in the capillary). Reproducing crystals under the same conditions in sitting drops was not successful probably because capillaries work on the principle of counter diffusion, which is strikingly different from vapour diffusion used in sitting or hanging drops in terms of the kinetics of equilibration and concentration used. Therefore, PEG 20K concentration was varied in a large range for forming crystals in sitting drops. Crystals with plate morphology were finally obtained in sitting drops (Figure 3B) with 4% PEG 20K, 100 mM Na HEPES, pH 7.5, and 50 mM KSCN in the reservoir. For crystal handling, mounting in loops (Figure 3C) and freezing, overnight stabilization with increasing PEG 20K in reservoir to 6 or 8% was tried, to stabilize crystals but resulted in no diffraction. Adding medium-sized PEGs such as PEG 4 K, 6 K or 8 K with or without glycerol, either resulted in no diffraction or did not improve diffraction. First diffraction spots up to 60 Å could be observed for small, thin and fragile crystals ($60 \times 10 \times 2$ μm, SLS beamline PX I) with 16% glycerol as cryo-protectant added directly into the crystallization drop. With notably larger crystals ($100 \times 50 \times 5$ μm) diffraction improved to 26 Å (at SLS beamline PX I) showing a full reciprocal lattice (Figure 3E). For this and all subsequent experiments, the cryo-protectant was increased in steps of 2–4% to prevent osmotic shock damage to the crystal. The sample stability under crystallization conditions was verified using ethidium bromide–stained agarose gels for presence of rRNA after 2–4 weeks of sample preparation (Figure 3D). The gel shows 18S and 28S rRNA bands, as do ribosomes that were stored at −80°C after preparation. A full data set could be collected to ∼40 Å resolution (Figure 3E and Table 2) from which the cell parameters, space group, Matthews coefficient, solvent content and number of molecules in the asymmetric unit could be derived (see below). Data were collected on a Pilatus detector at the SLS PX II beamline with a 10×30 μm or 10×50 μm X-ray beam and 0.2° oscillations, detector distance 1200 mm, wavelength 0.997 Å. Both 80S complexes with or without endogenous E-site tRNA, as characterized by cryo-EM (Figure 2), were used for crystallization assays. However, crystals grew only for ribosomes prepared at 150 mM KCl throughout, i.e., without any E-site tRNA washing step. This indicates that the crystals contain E-site tRNA, and that its presence could favor crystallization.

DISCUSSION

Human ribosomes represent an important target for structural studies because of health implications such as side effects of current antibiotics. While cryo-EM structures of human ribosomes have been recently reported to 4–5 Å resolution (18), no crystal structures are upcoming for now. Obtaining crystals of human ribosomes represents a major challenge, and any first clue on purification and crystallization conditions would be helpful, even if initial crystals usually diffract weakly. In a first strong effort in this direction, crystals of the human 80S ribosome were obtained using a nonstandard integrated structural biology approach, using a variety of established methods in a synergistic way rather than individually. This included establishing a detailed method for large-scale preparation of homogenous 80S ribosomes extracted from HeLa cells, which can be grown in large quantities and from which the ribosome purification is less complicated than from blood (18) or human placenta (29), majorly due to the ease of availability of HeLa cells and less tedious methods of initial lysis. Placenta handling requires immediate isolation of ribosomes, due to the inherent presence of large RNase contaminations; also, the lysis itself is tedious, requiring gauze filtration and dounce homogenizer owing to the presence of connective tissues. Similarly, blood samples require a ficoll-hypaque density-gradient centrifugation to separate out lymphocytes. Such extensive methods are not needed when handling HeLa cells: the usage of a detergent is sufficient for cell lysis without any additional purification step. Contaminants like

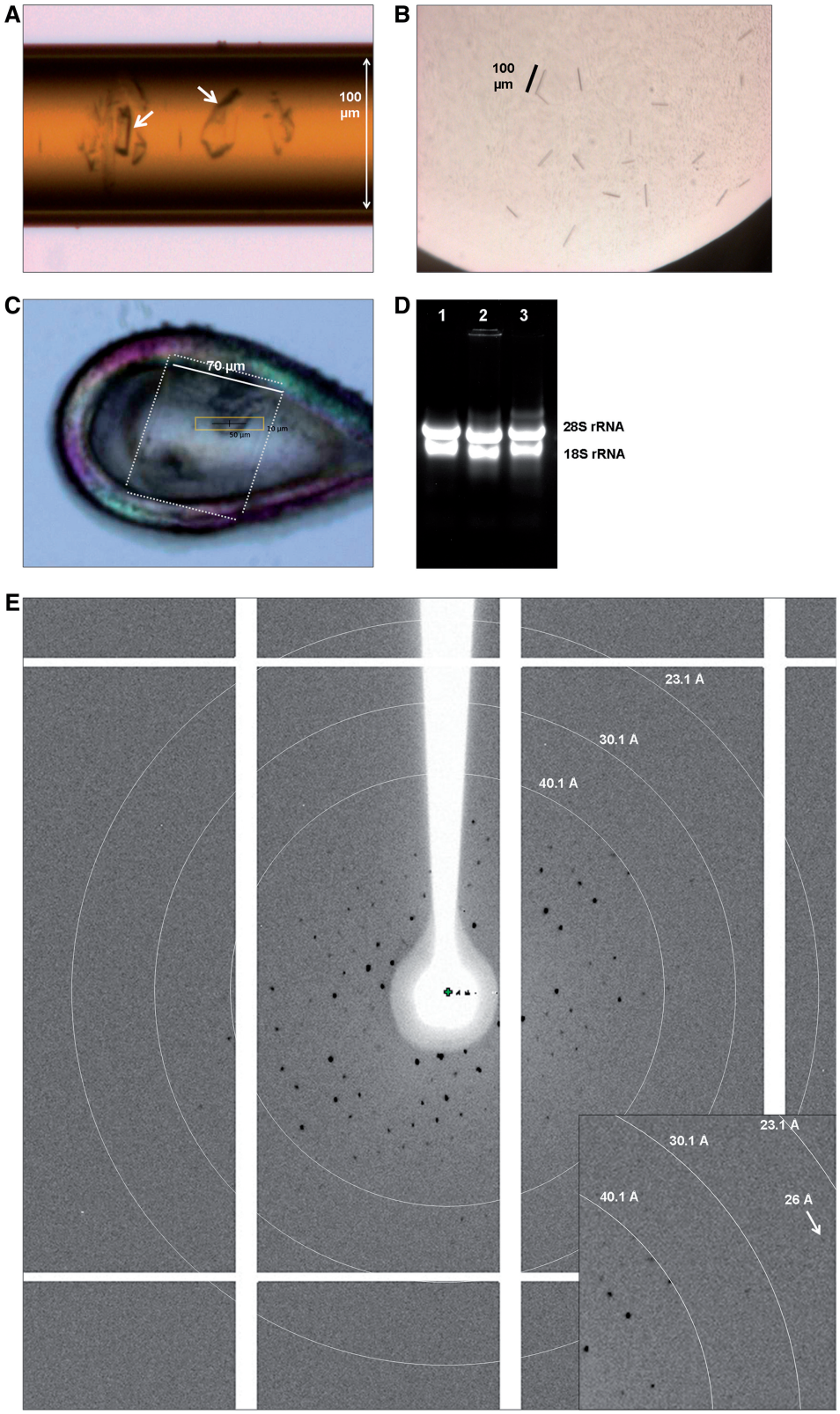

Figure 3. (**A**) First human 80S ribosome crystals obtained in the capillaries of a crystal harp. (**B**) Crystals with plate morphology reproduced in sitting drops that diffracted up to 26 Å, most are seen on the edge and thus give the impression of rods. (**C**) 80S crystal mounted in a cryogenic loop, tested for X-ray diffraction at the PX-II beamline at SLS. (**D**) Agarose gel depicting the sample stability under crystallization conditions as monitored by the presence of 18S and 28S rRNA. Lane 1 shows control ribosomes stored at −80°C, lanes 2 and 3 show ribosomes incubated with or without precipitant, respectively, for 4 weeks at 4°C. (**E**) The diffraction pattern shows a full reciprocal lattice with cell parameters of approximately a = 406 Å, b = 785 Å, c = 977 Å, with resolution rings indicated at 23, 30 and 40 Å. The inset shows diffraction spots extending to 26 Å resolution.

Table 2. Data collection statistics of a full data set collected from two regions of a single crystal at the SLS PX II beamline

X-ray data collection	Human 80S
Beamline	PX II (SLS)
Space group	C222(1)
Cell dimensions	
a, b, c (Å)	406.41, 784.99, 976.95
angles (°)	90, 90, 90
Resolution (Å)	150–42.0
Last shell	(43.9–42.0)
R_{sym} (%)	7.5 (74.1)
Reflections	5022
Completeness (%)	96.8 (88.6)
Redundancy	4.1 (3.2)
I/σ_i	7.7 (1.8)

Numbers in brackets refer to the highest resolution shell. R_{sym} is defined according to *XDS* (49).

ferritin in placenta are difficult to get rid of and tend to be co-purified with ribosomes. Ribosomes from HeLa cells analyzed in the present study neither have these contaminants nor these RNA and protein degradation issues known for placental ribosomes. The next two steps following cell lysis in the purification procedure are usually used for standard ribosome purifications: sucrose cushion and a gradient to obtain homogenous 80S ribosomes, which leads to an additional sucrose removal step. Here, human 80S were purified using PEG20K precipitation, which is a more straightforward method [used also for yeast ribosomes (7)]. The detailed standardized purification protocol described in this work is a prerequisite for structural studies of the human ribosome and has allowed obtaining first crystals that are highly reproducible from various cell culture batches. A typical feature of the work presented here is the biophysical characterization by SEC-MALLS, AUC and includes the usage of sucrose gradients. For example, SEC-MALLS and AUC helped to check the sample solubility and stability in different ionic conditions, along with molecular weight detection to check for presence of aggregates or dissociated subunits. Also, the exploration of various purification procedures, optimized by monitoring sample purity and homogeneity (in particular absence of aggregation) through direct nondenaturing cryo-EM visualization of the ribosome particles in conjunction with crystallization trials is a prominent feature of this work and has been the key in obtaining first 80S crystals, thanks to the unprecedented combined usage of cryo-EM and crystallography. Rather than performing a detailed structural analysis, cryo-EM was used for examining the sample composition (presence of structured rRNA's and ribosomal proteins, presence of tRNA's) and structural integrity from quickly obtainable medium-resolution cryo-EM maps (using data sets 10 times smaller than used for high-resolution structures reported previously) with the aim of obtaining crystallizable material. This structural analysis revealed the presence of E-site tRNA in human 80S ribosomes depending on a subtle difference in the purification protocol, that is the salt concentration used during Puromycin treatment. The salt-sensitivity suggests that this E-site tRNA binds in a nonspecific manner (50), probably also because no mRNA is present. This provides a valuable tool for obtaining either completely empty or E-site tRNA bound ribosomes, which can be used separately for further complex reconstitutions. For crystallization, we show that the presence of the E-site tRNA in human 80S ribosomes is helpful if not required because crystals could not be obtained with completely empty 80S ribosomes. This is probably because the E-site tRNA stabilizes the local ribosome structure, notably in the regions of the L1 and P-stalk proteins (51). The resulting conformation is compatible with the formation of inter-particle contacts in the crystal, as illustrated by the observed crystal nucleation and crystal growth, but different conformations may still be present in the asymmetric unit, as observed for yeast (7) and *T. thermophila* ribosomes (48). A related interesting aspect is that crystals can be obtained despite the presence of huge RNA ES elements, which protrude from the core structure (52); this is remarkable in terms of crystal packing, suggesting that ESs do not hamper crystallization in a significant way.

The use of capillaries for crystallization of large macromolecular complexes has been underexploited in the recent past, even though it is known to work well for smaller proteins (53,54). This work shows that unconventional methods like these can be helpful for initial screening of crystallization conditions, especially for inherently challenging samples and provide first hits to be further pursued in thicker capillaries or crystallization drops. The morphology of the human 80S ribosome crystals that form thin plates resembles that of early crystals of *T. thermophilus* ribosomes (55,56). After stabilization to reduce the fragile character of the thin crystals, they could be mounted in cryo loops in a rather straightforward manner. The crystals obtained diffract X-rays at a high-brilliance synchrotron source to up to 26 Å resolution, and show clear and fine diffraction spots along the reflection series of the diffraction pattern. The clean diffraction pattern also reveals that the crystals are monocrystalline, i.e. the crystal plates obtained under the crystallization conditions described here do not form multiple layers of distinct crystals, a phenomenon that otherwise occurs rather often for crystals with plate morphology. The diffraction pattern could be indexed, revealing that the crystals belong to the centric orthorhombic Bravais lattice type (space groups C222 or C2221, which have eight asymmetric units). The cell parameters of approximately a = 406 Å, b = 785 Å and c = 977 Å clearly indicate the presence of a large complex compatible with the Mw = 4.3 MDa estimated from the AUC and SEC-MALLS data. The calculation of the Matthews coefficient gives a value of $V_m = 3.0$ with three molecules in the asymmetric unit and a solvent content of 59%, or $V_m = 2.3$ with four molecules and 45% solvent [comparable with other ribosome crystals (57,58); the third alternative would give $V_m = 4.5$ with two molecules and a rather high solvent content of 73%]. The presence of three or four molecules in the asymmetric unit may be useful for noncrystallographic symmetry averaging, provided the ribosome

conformations are sufficiently similar. The small clean diffraction spots help in separating the spots and integrating the data, especially in the more challenging b- and c-directions. Because of the large cell parameters, fine-slicing was used with angular increments of 0.1–0.2° per frame in combination with a high-sensitivity and low readout noise pixel detector (Pilatus). In conclusion, the crystals are of excellent quality and diffraction data could be collected and processed, providing a first full data set at 42 Å resolution (Table 2). Their diffraction power, however, is limited (best resolution seen is 26 Å up to now, Figure 3E) most likely because of the little thickness of the crystals, which varies between 5 and 10 µm. In the future, it might be worth exploring conditions that promote crystal growth in the third dimension. Possibilities worth considering comprise further refined crystallization conditions such as the usage of additive screens and detergents, or removal of surface-exposed parts that may hamper further crystal growth such as loosely bound ribosomal proteins or part of the ES elements whose removal could help in obtaining larger crystals (some proteins could be removed by differential salt-wash as illustrated for the E-site tRNA, a procedure used for S1-removal; (59, 60) or cell line engineering such as done for L9-removal (61), which may be difficult to apply to human cells though. Although serum starvation was used (to synchronize cells), the ribosomes do not have any starvation factors bound, as compared with yeast ribosomes (7) or ribosomes isolated from blood (18), which have Stm-1 and Stm-1 like factors bound, respectively. This can be an advantage when forming translation complexes with mRNA and ribosomal translation factors for future crystallization or cryo-EM studies. Another aspect which we begun to analyze here is to refine the procedure for crystal stabilization and cryo-protection and reduce crystal mosaicity; controlled dehydration may also improve the diffraction of the crystals (7). In any case, while the crystals described here are diffracting relatively poorly and will need to be improved to reach a stronger diffraction power, they are the very first human ribosome crystals reported to our knowledge. This shows that the optimized purification procedure described herein provides crystallizable human ribosomes, a *sine-qua-non* condition for further crystallography work. The present work thus paves the way for future high-resolution crystal structures of the human ribosome, in isolated form or as complexes with mRNA, tRNAs and translation factors, with a major potential impact for studying molecular mechanisms and exploring medical applications in the ribosome field.

SUPPLEMENTARY DATA

Supplementary Data are available at NAR Online.

ACKNOWLEDGEMENTS

We would like to thank Meitian Wang and Florian Dworkowski from the Swiss Light Source for their excellent support on the PX I, II and III beamlines, Jean-Francois Ménétret for discussions on cryo-EM image processing and Betty Heller and Camille Apfel for support from the IGBMC cell culture facility, and the members of the IGBMC facilities, in particular the Structural Biology Platform, for their support. Authors contributions: H.K.: conception and design, experimental acquisition and interpretation of data, data processing, manuscript preparation; A.G.M.: cryo-EM data collection, image processing and analysis; L.M.: Hela cell cultures growth and maintenance; I.B.: acquisition and analysis of SEC-MALLS data; C.B.: acquisition of AUC data; S.S.: conception and design; B.P.K.: conception and design, crystal mounting, X-ray data processing, data analysis and manuscript preparation.

FUNDING

European Research Council (ERC Starting Grant N° 243296 TRANSLATIONMACHINERY); the Centre National pour la Recherche Scientifique (CNRS); French Infrastructure for Integrated Structural Biology (FRISBI) [ANR-10-INSB-05-01]; Instruct as part of the European Strategy Forum on Research Infrastructures (ESFRI); and Alsace Region, the Fondation pour la Recherche Médicale (FRM), INSERM, CNRS and the Association pour la Recherche sur le Cancer (ARC) (toward electron microscope facility). Funding for open access charge: ERC.

Conflict of interest statement. None declared.

REFERENCES

1. Dube,P., Bacher,G., Stark,H., Mueller,F., Zemlin,F., van Heel,M. and Brimacombe,R. (1998) Correlation of the expansion segments in mammalian rRNA with the fine structure of the 80 S ribosome; a cryoelectron microscopic reconstruction of the rabbit reticulocyte ribosome at 21 A resolution. *J. Mol. Biol.*, **279**, 403–421.
2. Chen,I.J., Wang,I.A., Tai,L.R. and Lin,A. (2008) The role of expansion segment of human ribosomal protein L35 in nuclear entry, translation activity, and endoplasmic reticulum docking. *Biochem. Cell Biol.*, **86**, 271–277.
3. Becker,T., Franckenberg,S., Wickles,S., Shoemaker,C.J., Anger,A.M., Armache,J.P., Sieber,H., Ungewickell,C., Berninghausen,O., Daberkow,I. *et al*. (2012) Structural basis of highly conserved ribosome recycling in eukaryotes and archaea. *Nature*, **482**, 501–506.
4. Klaholz,B.P. (2011) Molecular recognition and catalysis in translation termination complexes. *Trends Biochem. Sci.*, **36**, 282–292.
5. Jackson,R.J., Hellen,C.U. and Pestova,T.V. (2010) The mechanism of eukaryotic translation initiation and principles of its regulation. *Nat. Rev. Mol. Cell Biol.*, **11**, 113–127.
6. Klaholz,B.P., Myasnikov,A.G. and van Heel,M. (2004) Visualization of release factor 3 on the ribosome during termination of protein synthesis. *Nature*, **427**, 862–865.
7. Ben-Shem,A., Garreau de Loubresse,N., Melnikov,S., Jenner,L., Yusupova,G. and Yusupov,M. (2011) The structure of the eukaryotic ribosome at 3.0 A resolution. *Science*, **334**, 1524–1529.
8. Klinge,S., Voigts-Hoffmann,F., Leibundgut,M., Arpagaus,S. and Ban,N. (2011) Crystal structure of the eukaryotic 60S ribosomal subunit in complex with initiation factor 6. *Science*, **334**, 941–948.
9. Rabl,J., Leibundgut,M., Ataide,S.F., Haag,A. and Ban,N. (2011) Crystal structure of the eukaryotic 40S ribosomal subunit in complex with initiation factor 1. *Science*, **331**, 730–736.

10. Verschoor,A., Srivastava,S., Grassucci,R. and Frank,J. (1996) Native 3D structure of eukaryotic 80s ribosome: morphological homology with *E. coli* 70S ribosome. *J. Cell Biol.*, **133**, 495–505.
11. Armache,J.P., Jarasch,A., Anger,A.M., Villa,E., Becker,T., Bhushan,S., Jossinet,F., Habeck,M., Dindar,G., Franckenberg,S. *et al.* (2010) Cryo-EM structure and rRNA model of a translating eukaryotic 80S ribosome at 5.5-A resolution. *Proc. Natl Acad. Sci. USA*, **107**, 19748–19753.
12. Spahn,C.M., Jan,E., Mulder,A., Grassucci,R.A., Sarnow,P. and Frank,J. (2004) Cryo-EM visualization of a viral internal ribosome entry site bound to human ribosomes: the IRES functions as an RNA-based translation factor. *Cell*, **118**, 465–475.
13. Spahn,C.M., Beckmann,R., Eswar,N., Penczek,P.A., Sali,A., Blobel,G. and Frank,J. (2001) Structure of the 80S ribosome from Saccharomyces cerevisiae–tRNA-ribosome and subunit-subunit interactions. *Cell*, **107**, 373–386.
14. Chandramouli,P., Topf,M., Menetret,J.F., Eswar,N., Cannone,J.J., Gutell,R.R., Sali,A. and Akey,C.W. (2008) Structure of the mammalian 80S ribosome at 8.7 A resolution. *Structure*, **16**, 535–548.
15. Taylor,D., Unbehaun,A., Li,W., Das,S., Lei,J., Liao,H.Y., Grassucci,R.A., Pestova,T.V. and Frank,J. (2012) Cryo-EM structure of the mammalian eukaryotic release factor eRF1-eRF3-associated termination complex. *Proc. Natl Acad. Sci. USA*, **109**, 18413–18418.
16. Sengupta,J., Nilsson,J., Gursky,R., Spahn,C.M., Nissen,P. and Frank,J. (2004) Identification of the versatile scaffold protein RACK1 on the eukaryotic ribosome by cryo-EM. *Nat. Struct. Mol. Biol.*, **11**, 957–962.
17. Halic,M., Becker,T., Frank,J., Spahn,C.M. and Beckmann,R. (2005) Localization and dynamic behavior of ribosomal protein L30e. *Nat. Struct. Mol. Biol.*, **12**, 467–468.
18. Anger,A.M., Armache,J.P., Berninghausen,O., Habeck,M., Subklewe,M., Wilson,D.N. and Beckmann,R. (2013) Structures of the human and Drosophila 80S ribosome. *Nature*, **497**, 80–85.
19. Becker,T., Bhushan,S., Jarasch,A., Armache,J.P., Funes,S., Jossinet,F., Gumbart,J., Mielke,T., Berninghausen,O., Schulten,K. *et al.* (2009) Structure of monomeric yeast and mammalian Sec61 complexes interacting with the translating ribosome. *Science*, **326**, 1369–1373.
20. Taylor,D.J., Devkota,B., Huang,A.D., Topf,M., Narayanan,E., Sali,A., Harvey,S.C. and Frank,J. (2009) Comprehensive molecular structure of the eukaryotic ribosome. *Structure*, **17**, 1591–1604.
21. Becker,T., Armache,J.P., Jarasch,A., Anger,A.M., Villa,E., Sieber,H., Motaal,B.A., Mielke,T., Berninghausen,O. and Beckmann,R. (2011) Structure of the no-go mRNA decay complex Dom34-Hbs1 bound to a stalled 80S ribosome. *Nat. Struct. Mol. Biol.*, **18**, 715–720.
22. Hashem,Y., des Georges,A., Fu,J., Buss,S.N., Jossinet,F., Jobe,A., Zhang,Q., Liao,H.Y., Grassucci,R.A., Bajaj,C. *et al.* (2013) High-resolution cryo-electron microscopy structure of the Trypanosoma brucei ribosome. *Nature*, **494**, 385–389.
23. Yonath,A. (2005) Antibiotics targeting ribosomes: resistance, selectivity, synergism and cellular regulation. *Annu. Rev. Biochem.*, **74**, 649–679.
24. Franceschi,F. and Duffy,E.M. (2006) Structure-based drug design meets the ribosome. *Biochem. Pharmacol.*, **71**, 1016–1025.
25. Carter,A.P., Clemons,W.M., Brodersen,D.E., Morgan-Warren,R.J., Wimberly,B.T. and Ramakrishnan,V. (2000) Functional insights from the structure of the 30S ribosomal subunit and its interactions with antibiotics. *Nature*, **407**, 340–348.
26. Brodersen,D.E., Clemons,W.M. Jr, Carter,A.P., Morgan-Warren,R.J., Wimberly,B.T. and Ramakrishnan,V. (2000) The structural basis for the action of the antibiotics tetracycline, pactamycin, and hygromycin B on the 30S ribosomal subunit. *Cell*, **103**, 1143–1154.
27. Wilson,D.N., Harms,J.M., Nierhaus,K.H., Schlunzen,F. and Fucini,P. (2005) Species-specific antibiotic-ribosome interactions: implications for drug development. *Biol.Chem.*, **386**, 1239–1252.
28. Kannan,K. and Mankin,A.S. (2011) Macrolide antibiotics in the ribosome exit tunnel: species-specific binding and action. *Ann. N. Y. Acad. Sci.*, **1241**, 33–47.
29. Matasova,N.B., Myltseva,S.V., Zenkova,M.A., Graifer,D.M., Vladimirov,S.N. and Karpova,G.G. (1991) Isolation of ribosomal subunits containing intact rRNA from human placenta: estimation of functional activity of 80S ribosomes. *Anal. Biochem.*, **198**, 219–223.
30. Jan,E. and Sarnow,P. (2002) Factorless ribosome assembly on the internal ribosome entry site of cricket paralysis virus. *J. Mol. Biol.*, **324**, 889–902.
31. Tyulkina,L.G. and Mankin,A.S. (1984) Inhibition of ribonuclease contamination in preparations of T4 RNA ligase, polynucleotide kinase, and bacterial alkaline phosphatase with bentonite. *Anal. Biochem.*, **138**, 285–290.
32. Jacoli,G.G., Ronald,W.P. and Lavkulich,L. (1973) Inhibition of ribonuclease activity by bentonite. *Can. J. Biochem.*, **51**, 1558–1565.
33. Belin,S., Hacot,S., Daudignon,L., Therizols,G., Pourpe,S., Mertani,H.C., Rosa-Calatrava,M. and Diaz,J.J. (2010) Purification of ribosomes from human cell lines. *Curr. Protoc. Cell Biol.*, **Chapter 3**, Unit 3.40.
34. Blobel,G. and Sabatini,D. (1971) Dissociation of mammalian polyribosomes into subunits by puromycin. *Proc. Natl Acad. of Sci. USA*, **68**, 390–394.
35. Lebowitz,J., Lewis,M.S. and Schuck,P. (2002) Modern analytical ultracentrifugation in protein science: a tutorial review. *Protein Sci.*, **11**, 2067–2079.
36. Schuck,P. (2000) Size-distribution analysis of macromolecules by sedimentation velocity ultracentrifugation and lamm equation modeling. *Biophys. J.*, **78**, 1606–1619.
37. Ludtke,S.J., Baldwin,P.R. and Chiu,W. (1999) EMAN: semiautomated software for high-resolution single-particle reconstructions. *J. Struct. Biol.*, **128**, 82–97.
38. Tang,G., Peng,L., Baldwin,P.R., Mann,D.S., Jiang,W., Rees,I. and Ludtke,S.J. (2007) EMAN2: an extensible image processing suite for electron microscopy. *J. Struct. Biol.*, **157**, 38–46.
39. Saxton,W.O. and Baumeister,W. (1982) The correlation averaging of a regularly arranged bacterial cell envelope protein. *J. Microsc.*, **127**, 127–138.
40. Rosenthal,P.B. and Henderson,R. (2003) Optimal determination of particle orientation, absolute hand, and contrast loss in single-particle electron cryomicroscopy. *J. Mol. Biol.*, **333**, 721–745.
41. van Heel,M. and Schatz,M. (2005) Fourier shell correlation threshold criteria. *J. Struct. Biol.*, **151**, 250–262.
42. Kuwano,M., Endo,H. and Ikehera,Y. (1973) Differences in RNA formation and polyribosome metabolism in serum-starved normal and transformed cells. *Cancer Res.*, **33**, 2965–2971.
43. Grassucci,R.A., Taylor,D.J. and Frank,J. (2007) Preparation of macromolecular complexes for cryo-electron microscopy. *Nat. Protoc.*, **2**, 3239–3246.
44. Shenvi,C.L., Dong,K.C., Friedman,E.M., Hanson,J.A. and Cate,J.H. (2005) Accessibility of 18S rRNA in human 40S subunits and 80S ribosomes at physiological magnesium ion concentrations—implications for the study of ribosome dynamics. *RNA*, **11**, 1898–1908.
45. Moore,M.N. and Spremulli,L.L. (1985) Effects of cations and cosolvents on eukaryotic ribosomal subunit conformation. *Biochemistry*, **24**, 191–196.
46. Sperrazza,J.M., Russell,D.W. and Spremulli,L.L. (1980) Reversible dissociation of wheat germ ribosomal subunits: cation-dependent equilibria and thermodynamic parameters. *Biochemistry*, **19**, 1053–1058.
47. Beckmann,R., Spahn,C.M., Frank,J. and Blobel,G. (2001) The active 80S ribosome-Sec61 complex. *Cold Spring Harb. Symp. Quant. Biol.*, **66**, 543–554.
48. Weisser,M., Voigts-Hoffmann,F., Rabl,J., Leibundgut,M. and Ban,N. (2013) The crystal structure of the eukaryotic 40S ribosomal subunit in complex with eIF1 and eIF1A. *Nat. Struct. Mol. Biol.*, **20**, 1015–1017.
49. Kabsch,W. (2010) Xds. *Acta Crystallogr. D Biol. Crystallogr.*, **66**, 125–132.
50. Nierhaus,K.H. (2006) Decoding errors and the involvement of the E-site. *Biochimie*, **88**, 1013–1019.
51. Fei,J., Kosuri,P., MacDougall,D.D. and Gonzalez,R.L. Jr (2008) Coupling of ribosomal L1 stalk and tRNA dynamics during translation elongation. *Mol. Cell*, **30**, 348–359.

52. Melnikov,S., Ben-Shem,A., Garreau de Loubresse,N., Jenner,L., Yusupova,G. and Yusupov,M. (2012) One core, two shells: bacterial and eukaryotic ribosomes. *Nat. Struct. Mol. Biol.*, **19**, 560–567.
53. Lorber,B., Sauter,C., Theobald-Dietrich,A., Moreno,A., Schellenberger,P., Robert,M.C., Capelle,B., Sanglier,S., Potier,N. and Giege,R. (2009) Crystal growth of proteins, nucleic acids, and viruses in gels. *Prog. Biophys. Mol. Biol.*, **101**, 13–25.
54. Giege,R. and Sauter,C. (2010) Biocrystallography: past, present, future. *HFSP J.*, **4**, 109–121.
55. Yonath,A., Glotz,C., Gewitz,H.S., Bartels,K.S., von Bohlen,K., Makowski,I. and Wittmann,H.G. (1988) Characterization of crystals of small ribosomal subunits. *J. Mol. Biol.*, **203**, 831–834.
56. Yusupov,M.M., Yusupova,G.Z., Baucom,A., Lieberman,K., Earnest,T.N., Cate,J.H. and Noller,H.F. (2001) Crystal structure of the ribosome at 5.5 A resolution. *Science*, **292**, 883–896.
57. Gao,Y.G., Selmer,M., Dunham,C.M., Weixlbaumer,A., Kelley,A.C. and Ramakrishnan,V. (2009) The structure of the ribosome with elongation factor G trapped in the posttranslocational state. *Science*, **326**, 694–699.
58. Ben-Shem,A., Jenner,L., Yusupova,G. and Yusupov,M. (2010) Crystal structure of the eukaryotic ribosome. *Science*, **330**, 1203–1209.
59. Clemons,W.M. Jr, Brodersen,D.E., McCutcheon,J.P., May,J.L., Carter,A.P., Morgan-Warren,R.J., Wimberly,B.T. and Ramakrishnan,V. (2001) Crystal structure of the 30 S ribosomal subunit from Thermus thermophilus: purification, crystallization and structure determination. *J. Mol. Biol.*, **310**, 827–843.
60. Duval,M., Korepanov,A., Fuchsbauer,O., Fechter,P., Haller,A., Fabbretti,A., Choulier,L., Micura,R., Klaholz,B.P., Romby,P. *et al.* (2013) Escherichia coli Ribosomal Protein S1 Unfolds Structured mRNAs Onto the Ribosome for Active Translation Initiation. *PLoS Biol.*, **11**, e1001731.
61. Selmer,M., Gao,Y.G., Weixlbaumer,A. and Ramakrishnan,V. (2012) Ribosome engineering to promote new crystal forms. *Acta Crystallogr. D Biol. Crystallogr.*, **68**, 578–583.